Food Chemistry 455 (2024) 139773

Contents lists available at ScienceDirect

Food Chemistry

journal homepage: www.elsevier.com/locate/foodchem

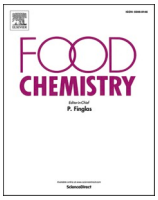

An advanced optic-fiber differential sensing system enhanced by molecularly imprinted polymer for specific sodium benzoate detection

Ze Xu [a], Li Jin [a], Bowen Yang [a], Wenwen Wang [a], Yukun Yang [b], Guanjun Wang [c], Jizhou Wu [a,d], Dandan Sun [a,*], Jie Ma [a,d,*]

[a] School of Physics and Electronic Engineering, Shanxi University, Taiyuan 030006, China
[b] School of Life Science, Shanxi University, Taiyuan 030006, China
[c] School of Information and Communication Engineering, Hainan University, Haikou 570228, China
[d] Collaborative Innovation Center of Extreme Optics, Shanxi University, Taiyuan 030006, China

ARTICLE INFO

Keywords:
Sodium benzoate
Microfiber interferometer
Fiber Bragg grating
Differential demodulation
Molecularly imprinted polymer
Food safety

ABSTRACT

A molecularly imprinted polymer (MIP) based microfiber differential demodulation sensing system for sodium benzoate (SB) concentration detection is proposed. The specific binding of MIP on the surface of microfibers with SB can lead to changes in local refractive index (RI). RI change induces a drift in the interference wavelength, which can be monitored by the power difference between two fiber Bragg gratings (FBGs). The sensing system can detect SB in the concentration range of 0.1–50 μg/ml, and interference wavelength and FBG power difference sensitivities are 0.55 nm/(μg/ml) and 2.64 dB/(μg/ml) in the low concentration range of 0.1–1 μg/ml, respectively, with a limit of detection (LOD) of 0.1 μg/ml. This microfiber differential demodulation sensing system is not only simple to fabricate, but also simplifies the demodulation equipment to reduce the cost, which providing a simple, reliable and low-cost technique for the quantitative detection of SB concentration in beverages and flavoured foods.

1. Introduction

With the changes in modern lifestyles, the food industry is increasingly using a variety of additives to improve food quality, color, aroma, taste and to extend the storage time of food products. (Bruna, Thais, & Lígia, 2018). Among these additives, preservatives are the most critical, which prolong food shelf life and inhibit spoilage (Zengin, Yuzbasioglu, Unal, Yilmaz, & Aksoy, 2011). As a preservative in a wide range of food products, sodium benzoate (SB) is classified by the US Food and Drug Administration (FDA) as a "Generally Recognised as Safe", which compound with a maximum permitted level of 0.1% in food (Lennerz et al., 2015). The Joint FAO/WHO Expert Committee on Food Additives (JECFA) has determined the Acceptable Daily Intake (ADI) for SB to be 0-5 mg per kilogram of body weight (Shahmohammadi, Javadi, & Nassiri-Asl, 2016; Zengin et al., 2011). Normal intake of SB in general population is not harmful to our body. However, excessive intake of SB has been linked to chromosomal abnormalities, non-immunization (pseudoallergy) in sensitized patients (Piper & Piper, 2017), DNA damage and increased micronucleus formation (Saatci et al., 2016), and hyperactivity (McCann et al., 2007). Moreover, SB may interact with other substances in some foods to produce harmful substances. For example, in some beverages, sodium benzoate may undergo a catalytic reaction with the free radicals of ascorbic acid, producing the carcinogenic substance benzene (Jacob, Hill, Lucero, & Nedorost, 2016; Piper, 2018). Therefore, the development of a sensitive, selective, simple and effective method for the determination of SB concentration in daily food is of great importance to human health.

Based on previous studies, several analytical techniques have been used to determine the concentration of SB. Fluorescence polarization immunoassay (FPIA) is used to determine SB in spiked samples (Ren et al., 2014). High performance liquid chromatography (HPLC) is used to determine SB in commercial lemonade and lemon butter samples (Dinc Zor, Asci, Aksu Donmez, & Yildirim Kucukkaraca, 2016) The SB preservative content of ibuprofen oral solution is detected by dispersive liquid-liquid microextraction (DLLME) coupled with surface enhanced Raman scattering (SERS) (Xue et al., 2020). Microfluidic colourimetric analysis (MCA) systems have been proposed for the determination of SB concentrations in common foods and beverages (Ko et al., 2021).

* Corresponding authors at: School of Physics and Electronic Engineering, Shanxi University, Taiyuan 030006, China.
E-mail addresses: sundd@sxu.edu.cn (D. Sun), mj@sxu.edu.cn (J. Ma).

https://doi.org/10.1016/j.foodchem.2024.139773
Received 20 January 2024; Received in revised form 29 April 2024; Accepted 19 May 2024
Available online 3 June 2024

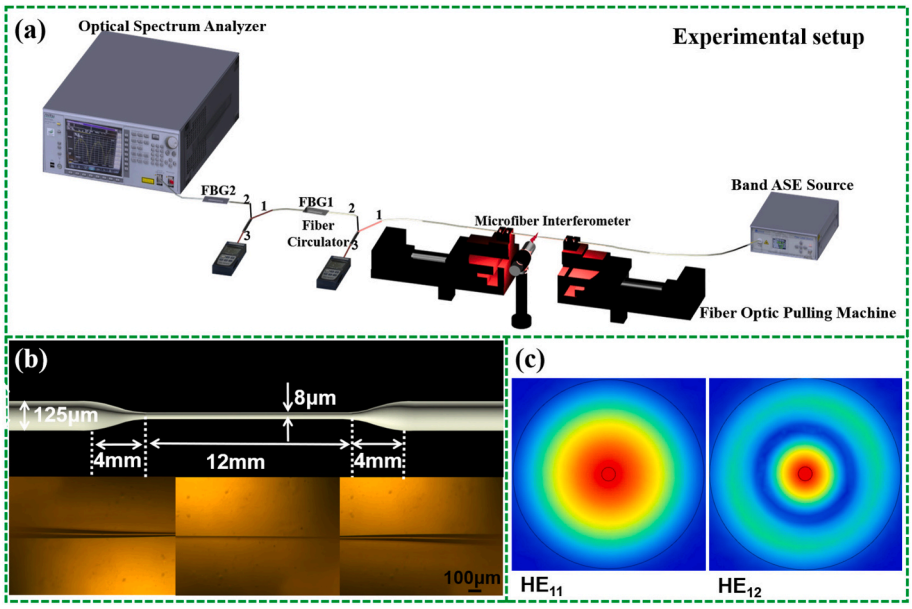

Fig. 1. (a) Schematic of the experimental setup (b) Schematic of the structure of the microfiber interferometer with parameters (c) The transverse electric field amplitude distributions for HE_{11} and HE_{12} in the major interference modes.

Molecularly imprinted polymer (MIP) piezoelectric sensors have been designed to detect SB concentrations in soft drinks (Zyablov & Vu Hoang, 2022). Kretschmann-based surface plasmon resonance (SPR) sensor is used to detect SB (Maurya & Verma, 2023). However, the above method, although effective in detecting SB, has some limitations. For example, FPIA requires complex pre-treatment and cryopreservation at −20 °C. The price and routine maintenance of HPLC are high, and the cost of analysis time and consumables is relatively high. The DLLME steps are more complicated. The wax-printed paper microchips used in the MCA system are susceptible to factors such as humidity, temperature, and light, which can affect the accuracy and stability of the piezoelectric sensors. Kretschmann-based SPR sensors are complex and require precious metal.

Based on the current state of research, optic-fiber sensing technology has emerged in order to develop a simple to fabricate, selective, stable and highly sensitive sensor. This technology has been widely researched and applied in industrial, environmental, and medical fields because of its light weight, small size, corrosion resistance, and high resistance to electromagnetic interference and radiation (Liu, Li, Zhang, & Zhao, 2021; P. Xiao et al., 2021). Currently, optic-fiber sensors have been implemented to sense temperature, magnetic field (Z. Hao, Pu, Lahoubi, Zhang, & Liu, 2023), pressure (J. Liu et al., 2022), pH (T. Liu, Wang, Ding, & Yi, 2019), heavy metal ions (Ma, Zheng, Zhang, Li, & Zhao, 2021; Y. Long, Li, Wang, Yang, & Liu, 2022; S.H.K. Yap et al., 2018; Samavati et al., 2022), and biomolecules (Lobry et al., 2023; W. Zheng, Zhang, Li, Li, & Zhao, 2022; Zheng et al., 2020; Y. Ran et al., 2022). As a potential sensing device, tapered microfiber has the unique advantages of high sensitivity, fast response time, compact size, and convenient configurability, as well as a large accessible evanescent fields (W. Luo, Chen, & Xu, 2021). Methyl parathion imprinted nanoparticles are fabricated and combined with a biconical microfiber interferometer to enable fine sensing of methyl parathion (Shrivastav, Sharma, & Jha, 2019). Polydopamine (PDA) is used as a molecularly imprinted material in combination with a microfiber interferometer to achieve the detection of C-responsive proteins (Liu et al., 2020). A highly sensitive optical sensor for the detection of urea is investigated, consisting of a microfiber interferometer integrated with an artificial MIP (Gorai & Jha, 2021). The molecular imprinting technique (MIT) in the above studies can generate template-shaped cavities with predetermined selectivity and high affinity in polymer matrices, which has been widely used in the field of sensing because of its good selectivity and stability (Chen, Xu, & Li, 2011). Based on the analysis of the above studies, combining MIT with tapered microfibers can bring into play their advantages sufficiently to achieve efficient, highly sensitive and specific detection of specific target molecules.

In this paper, a differential demodulation sensing system for the detection of sodium benzoate (SB) is designed by connecting a microfiber interferometer and fiber Bragg gratings (FBGs) to improve the estimation accuracy of the interferometer spectral offset by monitoring the variation of the FBG power difference. Notably, this unique design not only ensures simplicity in fabrication but also simplifies the demodulation device for effectively reducing overall costs. The experimental results show that the refractive index (RI) sensitivities of microfiber interferometer and FBG power difference are 1483 nm/RIU and 7450 dB/RIU, respectively, and the cross-temperature response can be obtained as low as −0.03 nm/°C and 0.09 dB/°C, respectively. Subsequent experimental analyses show that the sensing system has a significant response to SB in the range of 0.1–50 μg/ml in deionized water, with interference wavelength and FBG power difference sensitivities of 0.55 nm/(μg/ml) and 2.64 dB/(μg/ml), respectively, and the limit of detection (LOD) is calculated to be 0.1 μg/ml. Then, the sensing system is used to detect SB in sprite, soy sauce, and salad dressing. The investigated sensing system has the advantages of high sensitivity, good stability and easy operation, which makes it suitable as a screening tool for homogeneous detection of SB in daily foods.

2. Experimental section

2.1. Regents and instruments

Dopamine hydrochloride (DA) (98%), sodium benzoate (SB) (AR, 99.5%), acrylamide (AM) (99%), *N*,*N*′-methylenebisacrylamide (BIS) (AR), ammonium persulphate (APS) (AR, 98.5%), benzoic acid (BZ) (GC, ≥99.9%), potassium sorbate ($C_6H_7O_2K$) (≥99.0%), atrazine ($C_8H_{14}ClN_5$) (97%), sulfanilic acid ($C_6H_7NO_3S$) (AR,99.5%), 2-Chloro-2-phenylacetic acid ($C_8H_7ClO_2$) (96%), acetic acid (AC) (AR, 99.5%), sodium salicylate ($C_7H_5NaO_3$) (AR, 99.5%), tetramethylethylenediamine (TMEDA) (99%), sodium chloride (NaCl) (AR, 99.5%), phosphate buffer salinebuffer (PBS) (pH 7.2–7.4) and ethanol anhydrous (EtOH) (99.5%) are purchased from Shanghai Macklin Biochemical Technology Co., Ltd.

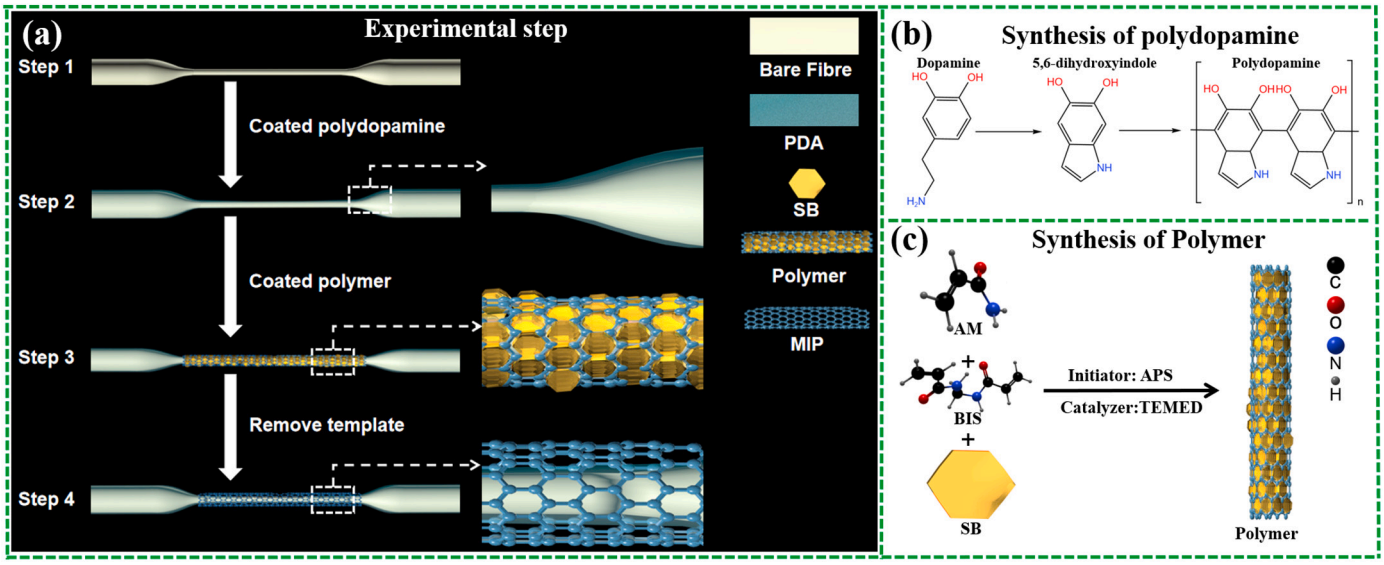

Fig. 2. (a) Schematic diagram of the functional steps of MIP microfiber interferometer (b) Schematic diagram of the principle of synthesising polydopamine (c) Schematic diagram of the principle of synthesising polymer.

(Shanghai, China). Tris-Hydrochloride Buffer (Tris-HCl) (pH 8.5) is bought from Aladdin Chemistry, Co., Ltd. (Shanghai, China). Sprite, soy sauce and salad dressing are purchased from supermarkets. Tris HCl buffer is used to dissolve DA. PBS buffer is used to dissolve AM and BIS, and deionized water (DI) is used to dissolve other reagents.

The optical experimental equipment includes a broadband light source (ASE, mchlight MCASE-CL-13-T-2-1-FA-T1, China), two optical power meters (OPM, China), two Bragg gratings (FBG, China), an optical spectral analyzer (OSA, Anritsu MS9740A, Japan), an optical fiber fusion splicer (FITEL, S178A, Japan), and a digital refractometer (Reichert 13,940,000, USA). The macrostructure of the microfiber interferometer is observed by an optical microscope (Caikon DMM—200C, China). An electrical shift stage controller (Zolix MC600, China) is used to fabricate the microfiber interferometer. A PR analytical balance (Ohaus, PR124ZH/E, China) is used to weigh the reagents. A column oven (HT-330, China) is utilized to perform temperature experiments. The equipments for the characterization experiments include a Fourier transform infrared spectrometer (FTIR, Thermo Nicolet iS5, USA), a scanning electron microscope (SEM, Zeiss Sigma300, Germany), and an energy spectrometer (EDS, Oxford Xplore30, Britain).

2.2. Experimental setup

As shown in Fig. 1 (a), the light source is emitted from the band ASE source (1528–1603 nm) with the power set to 10 dBm, passes through the microfiber interferometer to the port 1 of the circulator, and then passes through ports 2 and 3 of the optical circulator in order to reach the ports FBG1 and OPM2, respectively, and then passes through the other optical circulator, FBG2 and OPM2, and finally arrives at the OSA (600–1700 nm) with resolution 0.03 nm. The power changes of FBG1 and FBG2 are recorded by OPM1 and OPM2, respectively, and the interference spectral changes are recorded by the OSA.

2.3. Microfiber interferometer

2.3.1. Fabrication of microfiber interferometer

The fused biconical taper method is utilized to fabricate a microfiber interferometer. Firstly, an optical fiber fusion splicer is used to connect a middle section of photosensitive fiber in two sections of single-mode fiber. Then, the optical fiber is fixed with a fixture, and the photosensitive optical fiber is burned with a butane flame for 10 s. Finally, the optical fiber is uniformly stretched by the fiber optic pulling machine to obtain a microfiber interferometer. In order to minimize the experimental error, the stretching parameters are set to 2 mm/s for taper pulling speed, 5 mm/s^2 for acceleration, 9 mm/s for maximum speed, and 18 mm for taper pulling distance for each time. Fig. 1 (b, top) shows the specific parameters of the microfiber interferometer, which possess a uniform area with a length of 12 mm and a diameter of 8 μm and conical transition areas with a length of 4 mm. The structure of the microfiber interferometer is observed with an optical microscope as shown in Fig. 1 (b, bottom).

2.3.2. Principle of microfiber interferometer

Due to the special structure of the microfiber interferometer, when light passes through the first taper region, the diameter decreases, and the energy distribution of the fundamental mode cannot be changed fast enough, resulting in the leakage of the modes through the tapered region, while the energy loss of the fundamental mode is transformed into other higher-order modes with the same rotational symmetry (Bhardwaj, Kishor, & Sharma, 2020; Yap et al., 2018). The fundamental and higher-order modes will be transmitted simultaneously in the uniform region until a second taper region is reached. As the diameter becomes larger, the fundamental and higher order modes are coupled together (Bhardwaj et al., 2020). The fundamental mode (HE_{11}) and the first order higher-order mode (HE_{12}) represent the dominant mode coupling in the microfiber interferometer, because of the weak and negligible coupling between the fundamental mode and the other modes (Yap et al., 2018). Fig. 1 (c) shows the transverse electric field distribution of the fundamental mode (HE_{11}) and the higher-order mode (HE_{12}). Because the significant difference in effective RI exists in the modes of the microfiber interferometer, an interference pattern will appear (Ahsani, Ahmed, Jun, & Bradley, 2019). The output intensity of the interference pattern can be expressed as (Ahsani et al., 2019; Bhardwaj et al., 2020; Sun et al., 2019):

$$I = I_{C1} + I_{C2} + \sqrt{I_{C1} I_{C2}} cos\Delta\varphi \tag{1}$$

where I_{C1} and I_{C2} the intensities of the cladding and core modes, respectively. $\Delta\varphi$ is the phase difference between the two modes, denoted as (L.P. Sun et al., 2019):

$$\Delta\varphi = \frac{2\pi\Delta n_{eff} L_{eff}}{\lambda} \tag{2}$$

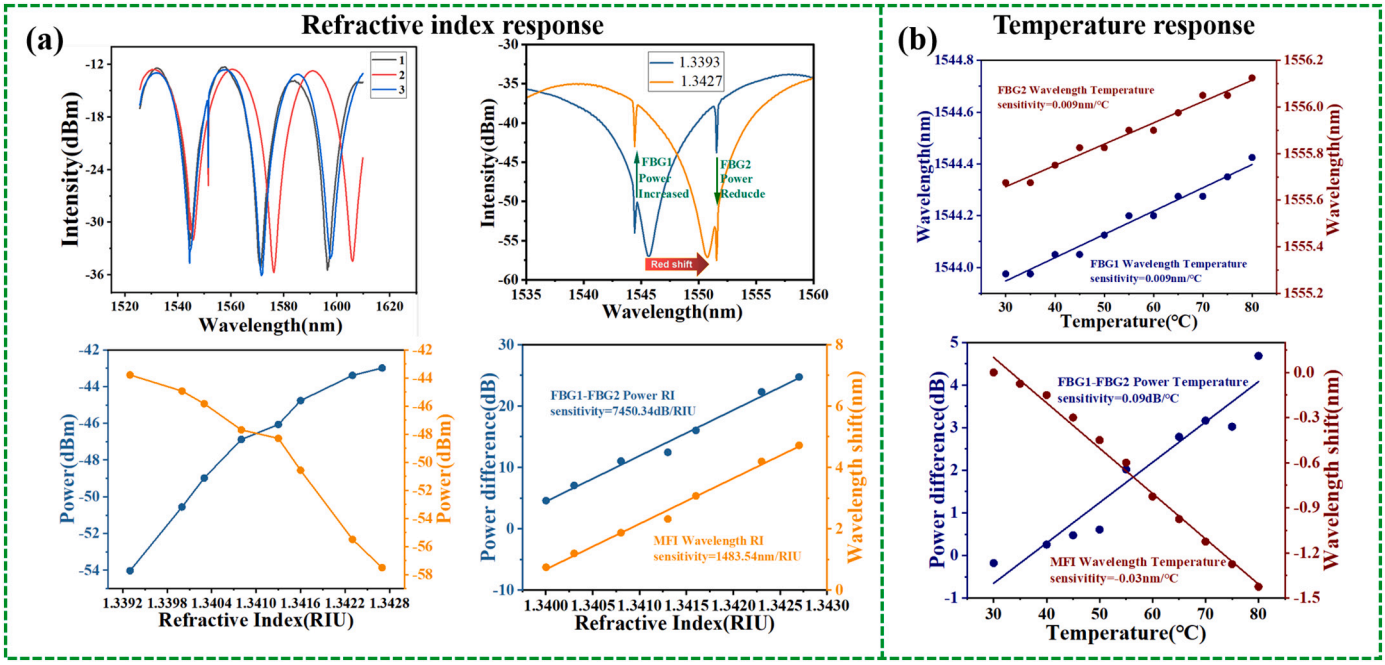

Fig. 3. (a) Interference spectra of three microfiber interferometers (top left), magnified view of the RI response of the interference wave (top right), Power variation of two FBGs (bottom left), RI response of the FBG power difference and the interference wavelength (bottom right) (b) Temperature response of two FBG wavelengths (top), Temperature response of the FBG power difference and the interference wavelength (bottom).

where Δn_{eff} is the difference between the fundamental mode and the high-order mode index, and L_{eff} is the length of the tapered area. λ is the input wavelength. By taking the partial derivative of the external refractive index from the input wavelength λ and using the phase difference $\Delta\varphi$, the interferometer refractive index sensitivity can be expressed as (Ahsani et al., 2019; Huang et al., 2015; Sun et al., 2019):

$$S = \frac{d\lambda}{dn_{med}} = \frac{\lambda}{\Gamma}\left(\frac{1}{\Delta neff}\frac{d\Delta neff}{dn_{med}}\right) \tag{3}$$

where $\Gamma = 1 - \frac{\lambda}{\Delta neff}\frac{d\Delta neff}{d\lambda}$ is the dispersion factor, which is usually negative value. dn_{med} is the RI variation of the surrounding medium. $\frac{d\Delta neff}{dn_{med}}$ is the exponential change due to small RI changes in the surrounding medium. From Eq. (3), the RI sensitivity S is mainly determined by λ, Γ, $\Delta neff$ and $\frac{d\Delta neff}{dn_{med}}$ together. However, the last three parameters are determined by the diameter of the microfiber interferometer (Sun et al., 2019). The smaller the diameter of the microfiber interferometer leads to a greater sensitivity because of the enhancement of the evanescent-field interaction and the reduction of the dispersion factor (Huang et al., 2015). The dip wavelength of the interference spectrum is red-shifted as the RI of the surrounding medium is increased (Sun, Fu, & Yang, 2020).

2.4. MIP microfiber sensor

2.4.1. Fabrication of MIP microfiber interferometer sensor

There are four steps to make the MIP microfiber interferometer sensor, as shown in Fig. 2 (a). In the first step, the microfiber interferometer is obtained by fused biconical taper method. In the second step, the microfiber immerses in the polydopamine (PDA) solution for 45 min to in-situ growth form a uniform PDA layer with super-adhesive properties on the microfiber surface. The initial PDA solution is prepared as follows: take 4 mg of DA, dissolve it in 2 ml of Tris-HCl to obtain a 2 mg/ml DA solution, and stir it for 5 min at room temperature, and the solution gradually turn into a gray color, which is successfully configured. In the third step, the microfiber with PDA coating on the surface is immersed in the polymeric solution for 20 min to allow the polymer layer to adhere to the surface of the PDA layer. The polymeric solution is prepared as follows: 0.5 g of template molecule SB is dissolved in 5 ml of DI. Then, 2 g of functional monomer AM and 0.1 g of cross-linker BIS are dissolved in 25 ml of PBS. Finally, 1 ml of the SB solution is mixed with 2 ml of AM/BIS solution, which dilutes to 10 ml with PBS solution. The ratio between the template molecule SB and the functional monomer AM is 10/3 mol. Then 0.25 μl of the catalyst TEMED and 0.02 g of the reaction initiator APS are added. The solution is stirred for 5 min at room temperature and allow to stand for 1 h to obtain the final polymeric solution. In the fourth step, microfibers with polymer and PDA on the surface are immersed in the elution solution for 5 min to remove the template molecule SB. The MIP microfiber sensor is washed with DI and dry for 30 min. The elution solution is obtained by mixing 9 ml of EtOH and 1 ml of AcOH.

2.4.2. Principle of MIP microfiber sensor

Dopamine is a small biological molecule structurally containing amine and catechol functional groups (Wang et al., 2014), which in can spontaneously form PDA by oxidative polymerization in alkaline solutions (pH > 7.5) (Hong et al., 2012). The polymerization process is shown in Fig. 2 (b), where dopamine is firstly oxidized to 5,6-dihydroxyindole (DHI) in Tris-HCl (pH 8.5), and then PDA is formed by non-covalent self-assembly and covalent polymerization (Hong et al., 2012). The reason why PDA have excellent adhesion is that it contain catecholamines, which can form covalent or non-covalent bonds (hydrogen bonds, π-π stacking forces) with the surface of the substrate material (Faure et al., 2013). The amino group contain in the polymer can be covalently coupled with the PDA active group, which makes the polymer firmly attach to the microfiber surface (Sabbagh & Muhamad, 2017; Sherwood, Xu, Lovas, Qin, & Bao, 2017; Wu et al., 2021; Yuan et al., 2017).

As shown in Fig. 2 (c), the template molecule SB, the monomer AM and the cross-linker BIS form stable polymers through non-covalent bonding interactions (hydrogen bonding, electrostatic attraction and weak interactions) under the initiation and catalysis of APS and TEMED (Verma & Gupta, 2013). Removal of the template molecule SB results in

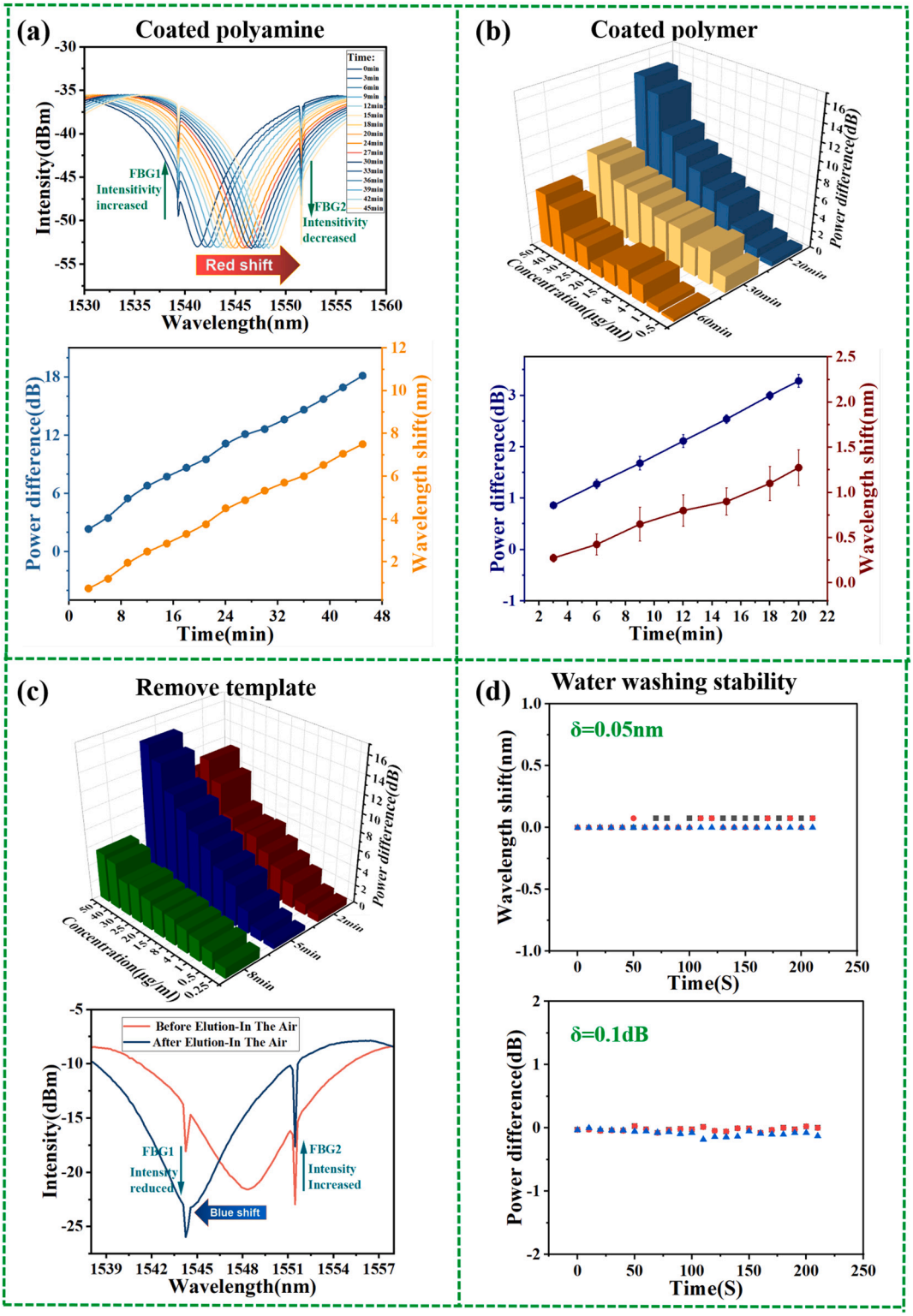

Fig. 4. (a) The spectrum of microfiber interferometer and FBGs for 45 min of immersion in polydopamine solution (top), The variation diagram of interference wavelength and FBG power difference (bottom) (b) Summary histogram of the detection response of MIP microfiber sensing probe for SB under different immersing times of polymeric solution (top), change of interference wavelength and FBG power difference over immersing time of 20 min (bottom) (c) Summary histogram of the detection response of the MIP microfiber sensing probe for SB under different removal times of the template (top), change of the interference wavelength before and after removing the template of 5 min (bottom) (d) Changes in wavelength shift (top) and FBG power difference (bottom) obtained from the spectra of MIP microfiber sensing probe recorded in DI.

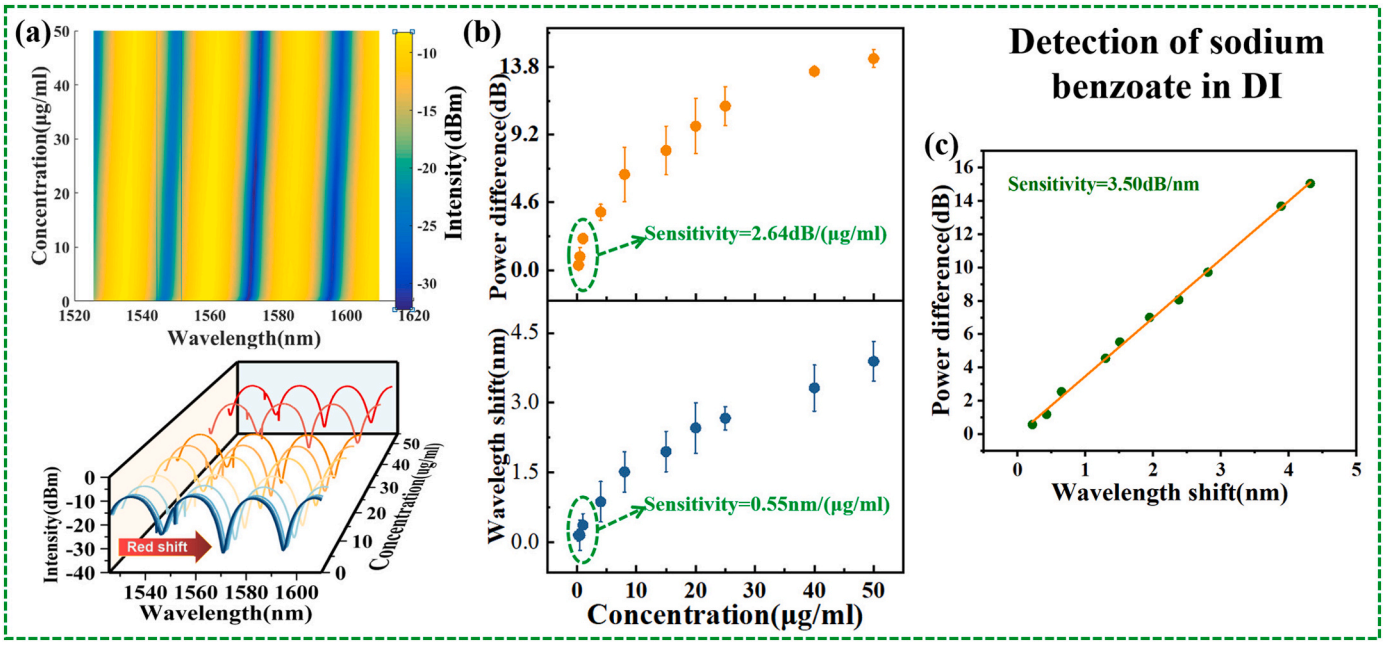

Fig. 5. (a) Interference spectral wavelength response of SB concentration detected by MIP microfiber sensing probe, corresponding to the displacement of the interference and grating spectrum (b) Interference wavelength and FBG power difference response of MIP microfiber sensing probe detecting SB concentration in the range of 0.1–50 μg/ml (c) Linear fitting plot of wavelength shift and FBG power difference.

the formation of specific binding sites on the polymer that are complementary in shape and size to the detectable substance (SB) (Chen et al., 2011). When SB is encountered again, the binding sites bind to it again by non-covalent bonding (Verma & Gupta, 2013). This results in an increase in the refractive index of the sensor surface.

3. Results and discussion

3.1. The performance of microfiber interferometer

The refractive index and temperature response of the microfiber interferometer are studied. Firstly, the RI solutions are prepared by dissolving NaCl in DI and then measured with a digital refractometer to produce solutions with refractive indices ranging from 1.3393 to 1.3427. As shown in Fig. 3 (a, top left), the spectra of three fabricated microfiber interferometers can be observed. For the RI experiment, the different RI solutions are dropped onto the surface of the microfiber interferometer, and the results are shown in Fig. 3 (a, top right). The higher the RI, the greater the red-shift of the interference wave, which leads to an increase in the peak power of FBG1 and a decrease in the peak power of FBG2. The peak power of the two FBGs are recorded by two optical power meters respectively, and their trends are shown in Fig. 3 (a, bottom left). Fig. 3 (a, bottom right) shows the interference wavelength RI sensitivity of 1483.54 nm/RIU and the FBG power difference RI sensitivity of 7450.34 dB/RIU. By detecting the variation of the FBG power difference, the estimation accuracy of the total spectral offset can be improved. A temperature experiment is conducted using a column oven, with a temperature setting of 30–80 °C. As the temperature increases, the interference wave undergoes a blue shift and the FBG wavelength undergoes a slight red shift, as shown in Fig. 3 (b, top). The temperature sensitivity is 0.009 nm/°C for both FBGs. Fig. 3 (b, bottom) shows the trend of the interference wave and the FBG power difference with temperature, with sensitivities of −0.03 nm/°C and 0.09 dB/°C, respectively.

3.2. Experimental results of the modification process

Fig. 4 (a, top) shows the variation of spectrum by immersing the microfiber interferometer in PDA solution for 45 min, and the gradual deposition of PDA causes the RI of the microfiber surface to become larger, which results in a wavelength red-shift of 8 nm and an increase of 11 dB in FBG power difference, as shown in Fig. 4 (a, bottom).

In order to obtain the best sensor sensitivity, the immersion time into the polymeric solution and the removal of the template are analyzed and optimised. The microfiber interferometers are immersed in the polymeric solution for 20 min, 30 min and 60 min, and the time for removing the template is kept as 5 min, and then the modified sensors are used to detect different concentrations of SB solution. Fig. 4 (b, top) shows that when immersing in the polymer solution for 20 min, 30 min, and 60 min, the FBG power difference changes by 15 dB, 8.5 dB, and 6.2 dB, respectively. If the immersion time of the polymeric solution is too short, too little polymer may be attached to the polydopamine layer, resulting in insufficient specific binding sites. When the immersion time of the polymeric solution is too long, it may cause the polymer layer on the microfiber surface to be too thick, which is not conducive a lower refractive index sensitivity, resulting in larger spectral losses. Therefore, the optimum time for immersion of the polymeric solution is finally chosen to be 20 min. As shown in Fig. 4 (b, bottom), the wavelength red-shift is about 1.5 nm and the FBG power difference is increased by about 3.5 dB within immersing 20 min in the polymeric solution.

Next, under maintaining the immersion time of 20 min in the polymeric solution, the removal times of the template are 2 min, 5 min, and 8 min respectively. These modified sensors are used to detect different concentrations of the SB solution. Fig. 4 (c, top) shows a FBG power difference of 10 dB for 2 min, 15 dB for 5 min and 5.5 dB for 8 min. When the remove template time is too short, it may result in template molecules in the polymer not being completely removed for leading to insufficient specific binding sites. When the remove template time for too long, it may result in washing away part of the microfiber surface PDA layer. As shown in Fig. 4 (c, bottom), there is a significant blue-shift in the interference wavelength after removing template molecules. Therefore, a final time of 20 min for immersion into the polymeric solution and 5 min for removal of template molecules is chosen.

The stability of this MIP microfiber sensing probe is verified by repeating the experiment three times to record the spectra of the MIP microfiber sensing probe in DI under the same steps and conditions to

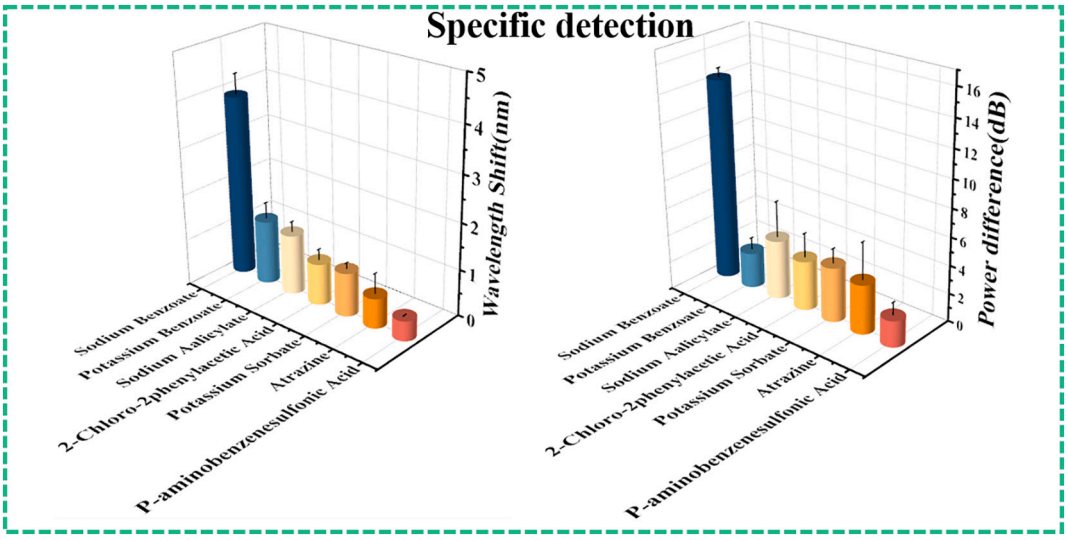

Fig. 6. Specific characteristics of the MIP microfiber sensor.

obtain the interferometric wavelength shifts and FBG power difference variations within the error range. As shown in Fig. 4 (d), it can be observed that the interference wavelength and the FBG power difference are basically stable with error fluctuations of 0.05 nm and 0.1 dB, respectively. Therefore, the fabricated MIP microfiber sensor is successful and can be used for further experiments.

3.3. Detection of sodium benzoate in DI

Firstly, SB powder is dissolved in DI to obtain SB solutions at concentrations of 0.1, 0.25, 0.5, 1, 4, 8, 15, 20, 25, 40, and 50 μg/ml. Then, it is detected sequentially from the lowest to the highest concentration using a MIP microfiber sensing probe. The blue area in Fig. 5 (a, top) indicates the shift in wavelength with increasing SB concentration. The macroscopic shift of the corresponding interference and grating spectrum is represented in Fig. 5 (a, bottom), where it can be seen that the interference spectrum shift in the direction of longer wavelengths. This is due to the fact that as the concentration of the SB solution increases, more and more numbers of SB molecules are bound by the specific binding sites, resulting in a larger refractive index on the fiber surface. Under the same experimental steps and conditions, the repeated experiments are conducted, and the trends of FBG power difference and wavelength of microfiber interferometer obtained by error analysis are shown in Fig. 5 (b). Upon reaching a detection concentration of up to 50 μg/ml, the wavelength undergoes a red-shift of approximately 4 nm, while the FBG power difference concurrently increases by about 14 dB. A fitting to the detection range spanning 0.1–1 μg/ml yields sensitivities of 0.55 nm/(μg/ml) for the wavelength shift and 2.64 dB/(μg/ml) for the FBG power difference. A linear relationship between wavelength shift and FBG power difference can be obtained from Fig. 5 (c), so the accuracy of wavelength estimation can be improved by calculating the FBG power difference. The limit of detection (LOD) be estimated as $\boldsymbol{LOD = 3\delta/S}$, where $\boldsymbol{\delta}$ is the grating standard deviation of 0.1 dB in the stability experiments and $\boldsymbol{S}$ is the sensitivity of the FBG power difference (Sun et al., 2020). The LOD is calculated to be 0.1 μg/ml.

3.4. Specific and stability detection

In order to validate the specificity of the MIP microfiber sensor, we performed three assays for several different substances (sodium benzoate, potassium benzoate, sodium salicylate, 2-chloro-2-phenylacetic acid, potassium sorbate, atrazine, and p-aminobenzenesulphonic acid) in the concentration range of 0–50 μg/ml. In Fig. 6 (left), the interference wavelengths are shown to be red-shifted by 4 nm, 1.3 nm, 1.2 nm, 0.8 nm, 0.9 nm, 0.6 nm and 0.4 nm, respectively. Fig. 6 (right) shows that the FBG power difference varied by 14 dB, 2.5 dB, 4.2 dB, 3.5 dB, 3.5 dB, 3.5 dB and 1.8 dB, respectively. To further investigate the specificity of the MIP microfiber sensor, the selectivity calculations for the imprinted molecule and competing molecules are carried out. k (selectivity coefficient) is calculated by the following equation $k = \Delta R_{template}/\Delta R_{competitor}$, where $\Delta R_{template}$ is the amount of change in FBG power difference for detecting the template molecule sodium benzoate and $\Delta R_{competitor}$ is the amount of change in FBG power difference for detecting the competing molecule (Chen, Xie, & Shi, 2013; Çimen, Bereli, & Denizli, 2021; Çimen, Bereli, Günaydın, & Denizli, 2022). As shown in Table 1, the selectivity of the MIP microfiber sensor for sodium benzoate is 3.33, 5.60, 4, 3.68, 4 and 7.78 times higher than that of sodium salicylate, potassium benzoate, 2-chloro-2-phenylacetic acid, potassium sorbate, atrazine and p-aminobenzenesulfonic acid, respectively. It can be obtained that the response of the MIP microfiber sensor to SB is much larger than that of other substances, indicating that this sensor has a better specific recognition effect on SB.

Table 1
Selectivity coefficients of competing molecules in MIP microfiber sensors.

Analyte	ΔR	k
sodium benzoate	14 dB	–
sodium salicylate	4.2 dB	3.33
2-chloro-2-phenylacetic acid	3.5 dB	4.00
potassium sorbate	3.8 dB	3.68
atrazine	3.5 dB	4.00
p-aminobenzenesulfonic acid	1.8 dB	7.78

In order to assess the stability of MIP microfiber sensors, the stability tests are carried out to monitor the stability and sensitivity of the manufactured MIP microfiber sensors over a long period of time. Measurements are taken over three different time periods: initially day 1, then day 5, and finally day 10, verifying the long-term performance under standard environmental conditions. Fig. 7 (a, top) shows the change in interference wavelength and FBG power difference after 200 s of immersion in DI for a sensor left at room temperature for one day. Fig. 7 (a, bottom) shows the fitted curves of interference wavelength and FBG power difference with concentration. Fig. 7 (b and c) shows the stability verification on day 5 and day 10, respectively. From the experimental data, it can be seen that the stability of the water washout of the sensing probe placed for different times remained basically the same (0.025 nm (day 1), 0.01 nm (day 5), and 0.025 nm (day 10)), and

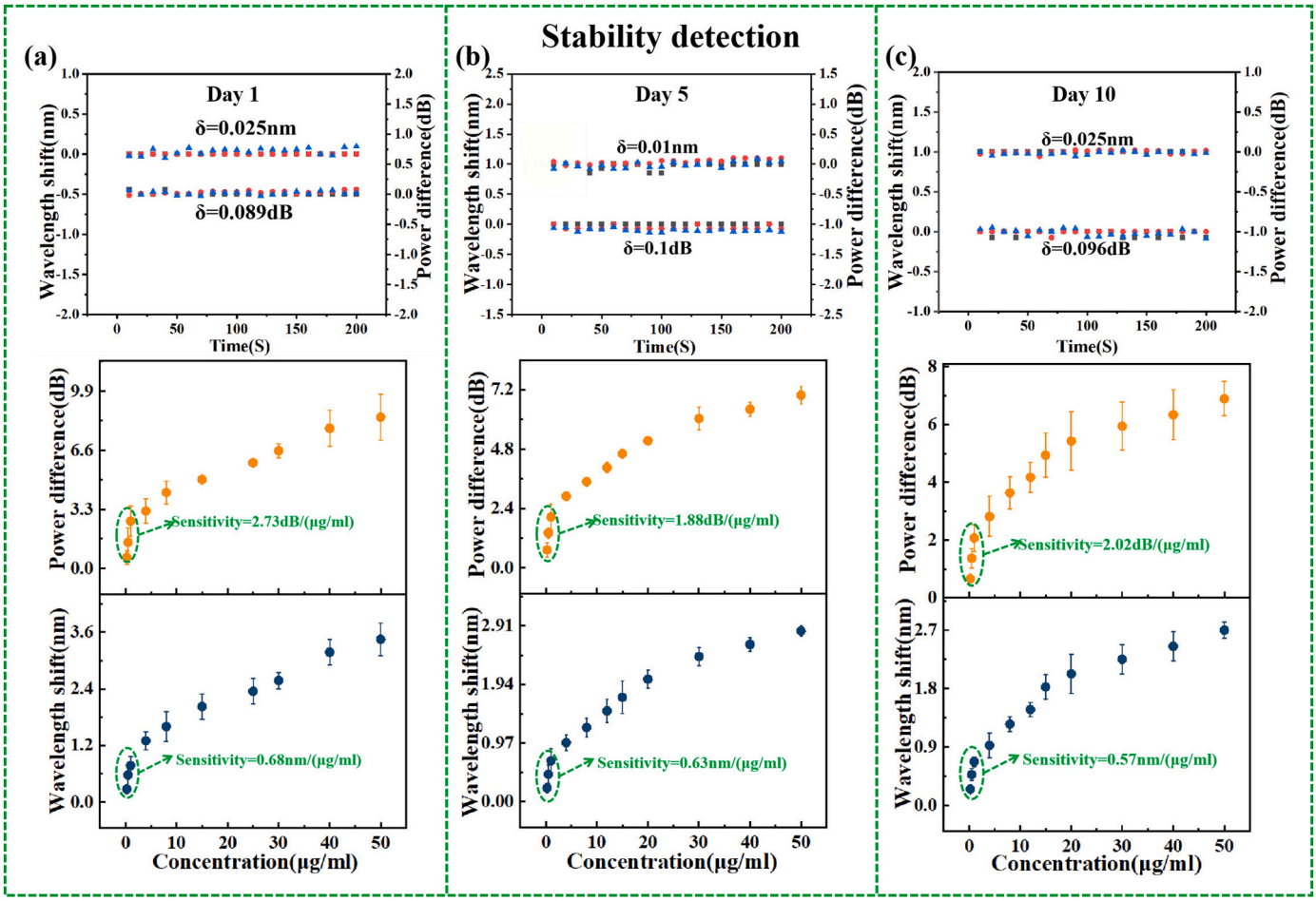

Fig. 7. (a) Stability detection of sensors placed at room temperature for 1 day (b) Stability detection of sensors placed at room temperature placed for 5 day (c) Stability detection of sensors placed at room temperature for 10 day.

the sensitivity of the interferometric wavelength shifts in the range of 0.1–1 μg/ml are 0.68 nm/(μg/ml) (day 1), 0.63 nm/(μg/ml) (day 5), 0.57 nm/(μg/ml) (day 10), and the FBG power difference sensitivities are 2.73 dB/(μg/ml) (day 1), 1.88 dB/(μg/ml) (day 5), and 2.02 dB/(μg/ml) (day 10), respectively. The experimental results show that the proposed MIP microfiber sensors have excellent stability. The sensor performance also can maintain the remarkable consistency when placed at room temperature conditions for 10 days.

3.5. Actual detection

To investigate the practical effectiveness of the MIP microfiber sensor, several foods (sprite, soy sauce, and salad dressing) each containing SB as an additive in their formulations are tested. The food samples are dissolved in DI and subjected to filtration. Subsequently, DI is added to prepare a 50 μg/ml stock solution. The solution is then further diluted with DI to give a series of gradient solutions at concentrations of 40, 30, 25, 20, 8, 4, 1, 0.5, 0.25 and 0.1 μg/ml, which are detected sequentially from the lowest to the highest concentration using the MIP microfiber sensor. Under the same experimental steps and conditions, some repetitions of the experiment are performed and error analyses are performed to obtain the trend of wavelength shift and FBG power difference. Fig. 8 (a) shows the spectrums of detecting SB in sprite, soy sauce, and salad dressing solutions from top to bottom. As the SB content increases, the interference spectrum undergoes a red-shift. From Fig. 8 (b), it can be seen that the interference wave are red-shifted by 3.5 nm, 3.5 nm and 3 nm in sprite, soy sauce and salad dressing, respectively, and the wavelength sensitivities in the fitted concentration range of 0.1–1 μg/ml are 0.66 nm/(μg/ml), 0.6 nm/(μg/ml) and 0.79 nm/(μg/ml), respectively. Fig. 8 (c) shows the variation of FBG power difference for the detection of SB in sprite, soy sauce and salad dressing solutions from top to bottom, which shows that the FBG power difference increases by 9.7 dB, 7.7 dB and 8 dB, respectively. The fitted FBG power difference sensitivities in the concentration range of 0.1–1 μg/ml are 1.92 dB/(μg/ml), 1.49 dB/(μg/ml) and 1.8 dB/(μg/ml), respectively. Fig. 8 (d) shows the linear fitting plots of wavelength shift and FBG power difference for sprite, soy sauce and salad dressing solutions from top to bottom, which can be obtained that there is a linear relationship between wavelength offset and FBG power difference, thus the method of improving the accuracy of wavelength estimation by FBG power difference is feasible. The experimental results show that the sensing system could be used to detect SB in daily food.

3.6. MIP microfiber sensors characterization

In order to verify feasibility and efficiency of this MIP sensing technology for successfully detecting SB, we analyse the FTIR spectrum on slides coated with PDA, PDA/Polymer, remove template and detected SB. As shown in Fig. 9 (a), the black line is the FTIR spectrum of PDA, and the absorption peaks near 3179 cm^{-1} in the black line are caused by O—H and N—H stretching vibrations (Yao et al., 2019), and the absorption peak near 2941 cm^{-1} is a C—H stretching vibration. The red line is the FTIR spectrum of PDA/polymer, and the increase in absorption intensity near 2941 cm^{-1} in the red line indicates the increase of C—H stretching vibration (Su et al., 2022), while the N—H bending vibration decays from 1629 cm^{-1} (black line) to 1627 cm^{-1} (red line),

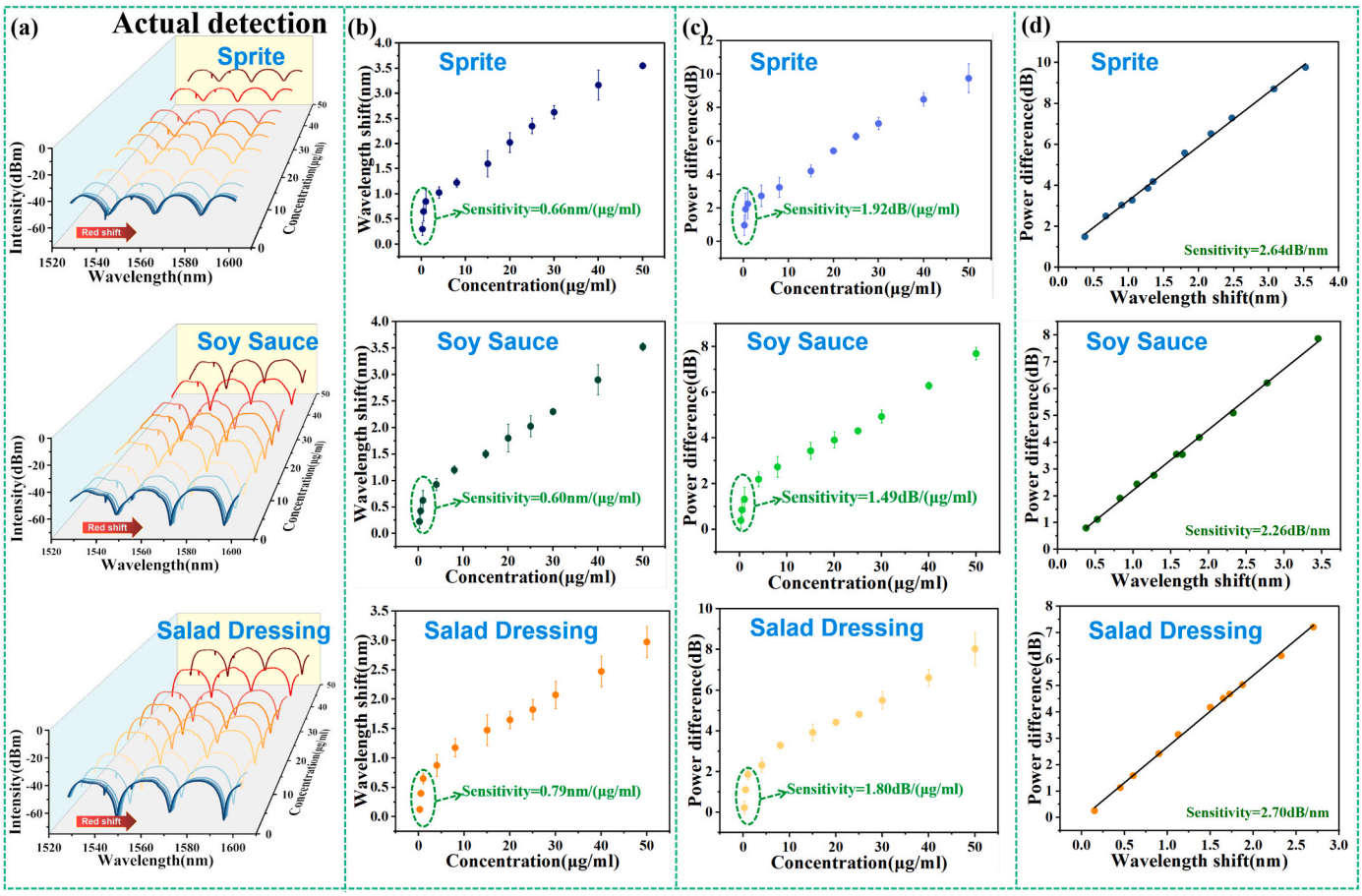

Fig. 8. (a) Interference spectral shifts for the actual detection of sprite, soy sauce and salad dressing (b) Interference wavelength response for the detection of SB concentration in the range of 0.1–50 μg/ml (c) FBG power difference response for the detection of SB concentration in the range of 0.1–50 μg/ml (d) Linear fit plot of wavelength shift and FBG power difference.

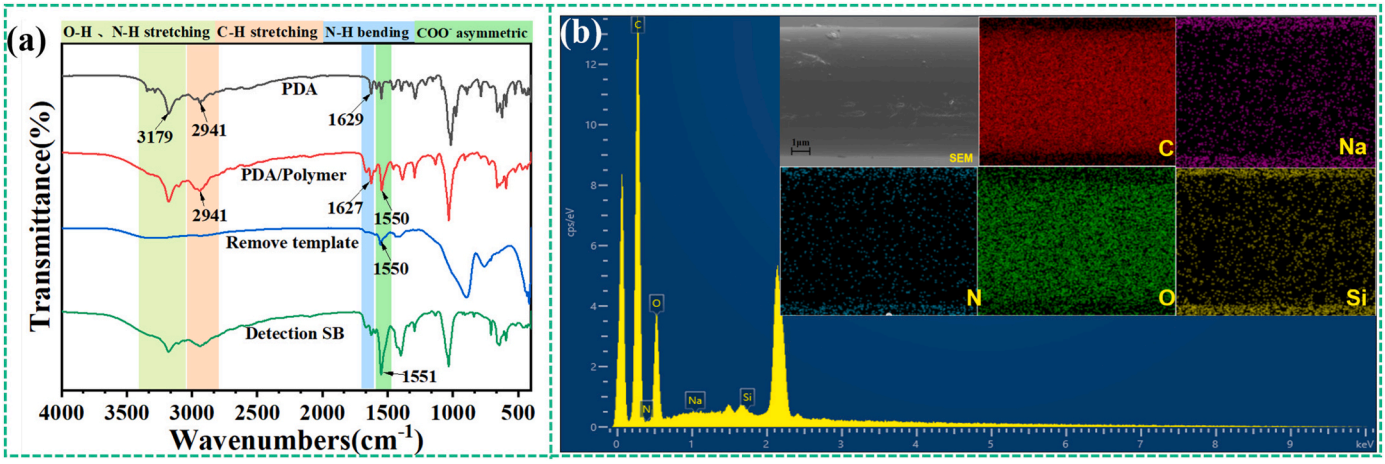

Fig. 9. (a) FTIR spectrum of PDA, PDA/Polymer, removal template and after detection of SB (b) EDS analysis of fiber surface after detection of SB (inset shows SEM characterization and mapping analysis of fiber surface).

which can indicate that the polymer has successfully adhered to the surface of the PDA (Su et al., 2022; Yao et al., 2019). The carboxylate anion of the SB vibrations stretch asymmetrically at 1550 cm^{-1} (red line) indicating both the successful attachment of the polymer to the PDA surface and the presence of the template molecule SB on the polymer surface (Kumar, Thomas, Tokas, & Kshirsagar, 2014). The blue line is the FTIR spectrum of the remove template, and the absorption intensity at 1550 cm^{-1} in the blue line becomes smaller, indicating that the template molecule SB has been removed. The green line is the FTIR spectrum after the detection of SB, and an increase in absorption intensity at 1551 cm^{-1} is observed (green line), indicating that SB has been recaptured.

Fig. 9 (b) shows the results of elemental analysis and the inset shows the SEM image of the fiber with functional layers, where it can be

Table 2
Comparison of SB detection methods.

Methods	Concentration Range	Sensitivity	LOD	Cost	Manufacturing difficulty	Publication Date
Fluorescence polarization immunoassay	0.3–20 μg/ml	–	0.26 μg/ml	High	difficulty	2014
High-performance liquid chromatography	5–30 μg/ml	–	0.154 μg/ml	High	easy	2016
Dispersive liquid-liquid microextraction combining surface enhanced Raman scattering	10–500 μg/ml	32.33 a.u./(μg/ml)	0.56 μg/ml	High	difficulty	2020
Microfluidic colorimetric analysis	50.4–5040 μg/ml	−0.034 a.u./ppm	50.4 μg/ml	High	medium	2021
MIP Piezoelectric	5–500 μg/ml	–	2 μg/ml	Medium	medium	2022
MIP Kretschmann-based surface plasmon resonance	0–40 μg/ml	2.93 nm/(μg/ml)	0.083 μg/ml	High	difficulty	2023
MIP microfiber interferometer and FBG	0.1–50 μg/ml	2.64 dB/(μg/ml)	0.1 μg/ml	Low	easy	This study

observed that a homogeneous sensing film is formed on the surface of the fiber. The mapping analysis shows the elements of C, O, Si, N and Na, respectively. O and Si are the constituent elements of the fiber material. The uniform distribution of the C and N elements indicates that the PDA and the polymer have been successfully attached to the fiber surface (Sureshkumar & Lee, 2011; Guo et al., 2019), and the uniform distribution of the Na element indicates that the fabricated sensor is able to successfully capture the SB.

Table 2 shows the comparison of this work with some popular methods currently used to detect SB concentration. In contrast, this proposed sensing system is not only simple and less expensive to fabricate, but also achieves more accurate detection of SB concentration in the low concentration range by detecting the interference wavelength drift and FBG power difference. The use of two Bragg gratings as a differential demodulation system simplifies demodulation equipment and reduces costs.

4. Conclusion

In this work, a differential demodulation system for the detection of sodium benzoate (SB) is fabricated by using a tapered fiber interferometer with molecularly imprinted polymer (MIP) film and two Bragg gratings, which simplifies demodulation equipment and reduces costs. The MIP coating captures the SB to cause a change in the refractive index of the fiber surface, which can be monitored by the interference wavelength drift and the FBG power difference. The RI sensitivity and cross-temperature response of the microfiber interferometer are 1483 nm/RIU and − 0.03 nm/°C, respectively. The RI sensitivity and cross-temperature response of the FBG power differential are 7450 dB/RIU and 0.09 dB/°C, respectively. The sensing system is able to effectively detect SB in the concentration range of 0.1–50 μg/ml, and the sensitivities of interference wavelength and FBG power difference are 0.55 nm/(μg/ml) and 2.64 dB/(μg/ml), respectively, in the low concentration range of 0.1–1 μg/ml, with a limit of detection (LOD) of 0.1 μg/ml. The experimental results show that the system can be used for the determination of SB in sprite, soy sauce and salad dressing. This sensing system is simple, low-cost, stable and sensitive, and has a very wide application potential in the field of food safety.

CRediT authorship contribution statement

Ze Xu: Writing – original draft, Methodology, Investigation, Data curation. **Li Jin:** Investigation, Data curation. **Bowen Yang:** Methodology, Data curation. **Wenwen Wang:** Methodology, Data curation. **Yukun Yang:** Methodology, Funding acquisition. **Guanjun Wang:** Project administration, Funding acquisition. **Jizhou Wu:** Supervision, Investigation, Funding acquisition. **Dandan Sun:** Writing – review & editing, Supervision, Project administration, Investigation. **Jie Ma:** Supervision, Project administration, Funding acquisition.

Declaration of competing interest

The authors declare that they have no known competing financial interests or personal relationships that could have appeared to influence the work reported in this paper.

Data availability

Data will be made available on request.

Acknowledgments

This work was supported by National Natural Science Foundation of China (62005147, U2341211, 32072301, 62175054, 62175140); International Cooperation and Exchange of the National Natural Science Foundation of China (62020106014).

References

Ahsani, V., Ahmed, F., Jun, M. B. G., & Bradley, C. (2019). Tapered fiber-optic Mach-Zehnder interferometer for ultra-high sensitivity measurement of refractive index. *Sensors, 19*(7). https://doi.org/10.3390/s19071652

Bhardwaj, V., Kishor, K., & Sharma, A. C. (2020). Tapered optical fiber geometries and sensing applications based on Mach-Zehnder interferometer: A review. *Optical Fiber Technology, 58*. https://doi.org/10.1016/j.yofte.2020.102302

Bruna, G. O. L., Thais, A. C. C., & Lígia, A. C. C. (2018). Food additives and their health effects: A review on preservative sodium benzoate. *African Journal of Biotechnology, 17*(10), 306–310. https://doi.org/10.5897/ajb2017.16321

Chen, F. F., Xie, X. Y., & Shi, Y. P. (2013). Preparation of magnetic molecularly imprinted polymer for selective recognition of resveratrol in wine. *Journal of Chromatography A, 1300*, 112–118. https://doi.org/10.1016/j.chroma.2013.02.018

Chen, L., Xu, S., & Li, J. (2011). Recent advances in molecular imprinting technology: Current status, challenges and highlighted applications. *Chemical Society Reviews, 40*(5), 2922–2942. https://doi.org/10.1039/c0cs00084a

Çimen, D., Bereli, N., & Denizli, A. (2021). Surface plasmon resonance based on molecularly imprinted polymeric film for L-phenylalanine detection. *Biosensors, 11*(1), 21. https://doi.org/10.3390/bios11010021

Dinc Zor, S., Asci, B., Aksu Donmez, O., & Yildirim Kucukkaraca, D. (2016). Simultaneous determination of potassium sorbate, sodium benzoate, Quinoline yellow and sunset yellow in lemonades and lemon sauces by HPLC using experimental design. *Journal of Chromatographic Science, 54*(6), 952–957. https://doi.org/10.1093/chromsci/bmw027

Faure, E., Falentin-Daudré, C., Jérôme, C., Lyskawa, J., Fournier, D., Woisel, P., & Detrembleur, C. (2013). Catechols as versatile platforms in polymer chemistry. *Progress in Polymer Science, 38*(1), 236–270. https://doi.org/10.1016/j.progpolymsci.2012.06.004

Gorai, P., & Jha, R. (2021). Artificial receptor-based optical sensors (AROS): Ultra-sensitive detection of urea. *Advanced Photonics Research, 2*(8). https://doi.org/10.1002/adpr.202100044

Guo, S., Li, Y., Wang, Y., Lu, Y., Wang, K., Bu, Y., … Huang, F. (2019). Bentonite-acrylamide hydrogels prepared by the nonmixing method: Characterization and properties. *ACS Omega, 4*(16), 16826–16832. https://doi.org/10.1021/acsomega.9b01630

Hao, Z., Pu, S., Lahoubi, M., Zhang, C., & Liu, W. (2023). Dual-channel-in-one temperature-compensated all-fiber-optic vector magnetic field sensor based on

surface plasmon resonance. *Optics Express, 31*(3), 4826–4838. https://doi.org/10.1364/OE.481161
Hong, S., Na, Y. S., Choi, S., Song, I. T., Kim, W. Y., & Lee, H. (2012). Non-covalent self-assembly and covalent polymerization co-contribute to polydopamine formation. *Advanced Functional Materials, 22*(22), 4711–4717. https://doi.org/10.1002/adfm.201201156
Huang, Y., Tian, Z., Sun, L. P., Sun, D., Li, J., Ran, Y., & Guan, B. O. (2015). High-sensitivity DNA biosensor based on optical fiber taper interferometer coated with conjugated polymer tentacle. *Optics Express, 23*(21), 26962–26968. https://doi.org/10.1364/OE.23.026962
Jacob, S. E., Hill, H., Lucero, H., & Nedorost, S. (2016). Benzoate allergy in children-from foods to personal hygiene products. *Pediatric Dermatology, 33*(2), 213–215. https://doi.org/10.1111/pde.12759
Ko, C. H., Liu, C. C., Chen, K. H., Sheu, F., Fu, L. M., & Chen, S. J. (2021). Microfluidic colorimetric analysis system for sodium benzoate detection in foods. *Food Chemistry, 345*, Article 128773. https://doi.org/10.1016/j.foodchem.2020.128773
Kumar, N., Thomas, S., Tokas, R. B., & Kshirsagar, R. J. (2014). Investigation on the adsorption characteristics of sodium benzoate and taurine on gold nanoparticle film by ATR-FTIR spectroscopy. *Spectrochimica Acta Part A: Molecular and Biomolecular Spectroscopy, 118*, 614–618. https://doi.org/10.1016/j.saa.2013.09.014
Lennerz, B. S., Vafai, S. B., Delaney, N. F., Clish, C. B., Deik, A. A., Pierce, K. A., … Mootha, V. K. (2015). Effects of sodium benzoate, a widely used food preservative, on glucose homeostasis and metabolic profiles in humans. *Molecular Genetics and Metabolism, 114*(1), 73–79. https://doi.org/10.1016/j.ymgme.2014.11.010
Liu, J., Hou, Y., Wang, J., Zhong, G., Zhang, L., Zhuang, F., … Wang, S. (2022). Multi-parameter demodulation for temperature, salinity and pressure sensor in seawater based on the semi-encapsulated microfiber Mach-Zehnder interferometer. *Measurement, 196*. https://doi.org/10.1016/j.measurement.2022.111213
Liu, T., Wang, W., Ding, H., & Yi, D. (2019). Smartphone-based hand-held optical fiber fluorescence sensor for on-site pH detection. *IEEE Sensors Journal, 19*(20), 9441–9446. https://doi.org/10.1109/jsen.2019.2926153
Liu, X., Lin, W., Xiao, P., Yang, M., Sun, L. P., Zhang, Y., … Guan, B. O. (2020). Polydopamine-based molecular imprinted optic microfiber sensor enhanced by template-mediated molecular rearrangement for ultra-sensitive C-reactive protein detection. *Chemical Engineering Journal, 387*. https://doi.org/10.1016/j.cej.2020.124074
Liu, Y., Li, X., Zhang, Y. N., & Zhao, Y. (2021). Fiber-optic sensors based on Vernier effect. *Measurement, 167*. https://doi.org/10.1016/j.measurement.2020.108451
Lobry, M., Loyez, M., Debliquy, M., Chah, K., Goormaghtigh, E., & Caucheteur, C. (2023). Electro-plasmonic-assisted biosensing of proteins and cells at the surface of optical fiber. *Biosensors and Bioelectronics, 220*, Article 114867. https://doi.org/10.1016/j.bios.2022.114867
Long, Y., Li, H., Wang, W., Yang, X., & Liu, Z. (2022). Ultrasensitive detection of Cr(VI) using a novel SERS optical fiber probe modified by dual-functional methimazole. *Journal of Alloys and Compounds, 910*. https://doi.org/10.1016/j.jallcom.2022.164916
Luo, W., Chen, Y., & Xu, F. (2021). Recent progress in microfiber-optic sensors. *Photonic Sensors, 11*(1), 45–68. https://doi.org/10.1007/s13320-021-0614-9
Ma, Y., Zheng, W., Zhang, Y.-N., Li, X., & Zhao, Y. (2021). Optical fiber SPR sensor with surface ion imprinting for highly sensitive and highly selective Ni^{2+} detection. *IEEE Transactions on Instrumentation and Measurement, 70*, 1–6. https://doi.org/10.1109/tim.2021.3107052
Maurya, P., & Verma, R. (2023). MIP integrated surface plasmon resonance in vitro detection of sodium benzoate. *Analyst, 148*(5), 1141–1150. https://doi.org/10.1039/d2an01910h
McCann, D., Barrett, A., Cooper, A., Crumpler, D., Dalen, L., Grimshaw, K., & Stevenson, J. (2007). Food additives and hyperactive behaviour in 3-year-old and 8/9-year-old children in the community: A randomised, double-blinded, placebo-controlled trial. *The Lancet, 370*(9598), 1560–1567. https://doi.org/10.1016/S0140-6736(07)61306-3
Piper, J. D., & Piper, P. W. (2017). Benzoate and sorbate salts: A systematic review of the potential hazards of these invaluable preservatives and the expanding spectrum of clinical uses for sodium benzoate. *Comprehensive Reviews in Food Science and Food Safety, 16*(5), 868–880. https://doi.org/10.1111/1541-4337.12284
Piper, P. W. (2018). Potential safety issues surrounding the use of benzoate preservatives. *Beverages, 4*(2), 33. https://doi.org/10.3390/beverages4020033
Ran, Y., Xu, Z., Chen, M., Wang, W., Wu, Y., Cai, J., … Guan, B. O. (2022). Fiber-optic theranostics (FOT): Interstitial fiber-optic needles for cancer sensing and therapy. *Advanced Science, 9*(15), Article e2200456. https://doi.org/10.1002/advs.202200456
Ren, L., Meng, M., Wang, P., Xu, Z., Eremin, S. A., Zhao, J., … Xi, R. (2014). Determination of sodium benzoate in food products by fluorescence polarization immunoassay. *Talanta, 121*, 136–143. https://doi.org/10.1016/j.talanta.2013.12.035
Saatci, C., Erdem, Y., Bayramov, R., Akalın, H., Tascioglu, N., & Ozkul, Y. (2016). Effect of sodium benzoate on DNA breakage, micronucleus formation and mitotic index in peripheral blood of pregnant rats and their newborns. *Biotechnology and Biotechnological Equipment, 30*(6), 1179–1183. https://doi.org/10.1080/13102818.2016.1224979
Sabbagh, F., & Muhamad, I. I. (2017). Physical and chemical characterisation of acrylamide-based hydrogels, Aam, Aam/NaCMC and Aam/NaCMC/MgO. *Journal of Inorganic and Organometallic Polymers and Materials, 27*(5), 1439–1449. https://doi.org/10.1007/s10904-017-0599-4
Samavati, Z., Samavati, A., Fauzi Ismail, A., Sohaimi Abdullah, M., Othman, H. D., & M.. (2022). Selective ultrasensitive FBG-SBL chemosensor for detection of copper ions in water resources based on plasmon resonance energy transfer. *Optics & Laser Technology, 153*. https://doi.org/10.1016/j.optlastec.2022.108289
Shahmohammadi, M., Javadi, M., & Nassiri-Asl, M. (2016). An overview on the effects of sodium benzoate as a preservative in food products. *Biotechnology and Health Sciences, 3*(3). https://doi.org/10.17795/bhs-35084
Sherwood, J., Xu, Y., Lovas, K., Qin, Y., & Bao, Y. (2017). Surface functionalization of dopamine coated iron oxide nanoparticles for various surface functionalities. *Journal of Magnetism and Magnetic Materials, 427*, 220–224. https://doi.org/10.1016/j.jmmm.2016.10.039
Shrivastav, A. M., Sharma, G., & Jha, R. (2019). Hypersensitive and selective biosensing based on microfiber interferometry and molecular imprinted nanoparticles. *Biosensors and Bioelectronics, 141*, Article 111347. https://doi.org/10.1016/j.bios.2019.111347
Su, J., Zhang, L., Wan, C., Deng, Z., Wei, S., Yong, K. T., & Wu, Y. (2022). Dual-network self-healing hydrogels composed of graphene oxide@nanocellulose and poly(AAm-co-AAc). *Carbohydrate Polymers, 296*, Article 119905. https://doi.org/10.1016/j.carbpol.2022.119905
Sun, D., Fu, Y., & Yang, Y. (2020). Label-free detection of breast cancer biomarker using silica microfiber interferometry. *Optics Communications, 463*. https://doi.org/10.1016/j.optcom.2020.125375
Sun, L. P., Huang, T., Yuan, Z., Lin, W., Xiao, P., Yang, M., … Guan, B. O. (2019). Ultra-high sensitivity of dual dispersion turning point taper-based Mach-Zehnder interferometer. *Optics Express, 27*(16), 23103–23111. https://doi.org/10.1364/OE.27.023103
Sureshkumar, M., & Lee, C. K. (2011). Polydopamine coated magnetic-chitin (MCT) particles as a new matrix for enzyme immobilization. *Carbohydrate Polymers, 84*(2), 775–780. https://doi.org/10.1016/j.carbpol.2010.03.036
Verma, R., & Gupta, B. D. (2013). Fiber optic SPR sensor for the detection of 3-pyridinecarboxamide (vitamin B3) using molecularly imprinted hydrogel. *Sensors and Actuators B: Chemical, 177*, 279–285. https://doi.org/10.1016/j.snb.2012.10.135
Wang, C., Zhu, W., Lan, Y., Zhang, M., Tian, T., Wang, H., & Li, G. (2014). Facile fabrication of reactive plasmonic substrates for fluorescence enhancement via mussel-inspired chemistry. *The Journal of Physical Chemistry C, 118*(20), 10754–10763. https://doi.org/10.1021/jp500384e
Wu, Y., Chen, X., Wang, X., Yang, M., Xu, F., Hou, C., & Huo, D. (2021). A fluorescent biosensor based on prismatic hollow metal-polydopamine frameworks and 6-carboxyfluorescein (FAM)-labeled protein aptamer for CA15-3 detection. *Sensors and Actuators B: Chemical, 329*. https://doi.org/10.1016/j.snb.2020.129249
Xiao, P., Xu, Z., Hu, D., Liang, L., Sun, L., Li, J., & Guan, B. O. (2021). Efficiently writing Bragg grating in high-birefringence elliptical microfiber for label-free immunosensing with temperature compensation. *Advanced Fiber Materials, 3*(5), 321–330. https://doi.org/10.1007/s42765-021-00087-7
Xue, L., Chen, L., Dong, J., Cai, L., Wang, Y., & Chen, X. (2020). Dispersive liquid-liquid microextraction coupled with surface enhanced Raman scattering for the rapid detection of sodium benzoate. *Talanta, 208*, Article 120360. https://doi.org/10.1016/j.talanta.2019.120360
Yao, J., Wu, T., Sun, Y., Ma, Z., Liu, M., Zhang, Y., & Yao, S. (2019). A novel biomimetic nanoenzyme based on ferrocene derivative polymer NPs coated with polydopamine. *Talanta, 195*, 265–271. https://doi.org/10.1016/j.talanta.2018.11.069
Yap, S. H. K., Chien, Y. H., Tan, R., Bin Shaik Alauddin, A. R., Ji, W. B., Tjin, S. C., & Yong, K. T. (2018). An advanced hand-held microfiber-based sensor for ultrasensitive Lead ion detection. *ACS Sensors, 3*(12), 2506–2512. https://doi.org/10.1021/acssensors.8b01031
Yuan, J., Zhang, Z., Yang, M., Guo, F., Men, X., & Liu, W. (2017). Surface modification of hybrid-fabric composites with amino silane and polydopamine for enhanced mechanical and tribological behaviors. *Tribology International, 107*, 10–17. https://doi.org/10.1016/j.triboint.2016.11.013
Zengin, N., Yuzbasioglu, D., Unal, F., Yilmaz, S., & Aksoy, H. (2011). The evaluation of the genotoxicity of two food preservatives: Sodium benzoate and potassium benzoate. *Food and Chemical Toxicology, 49*(4), 763–769. https://doi.org/10.1016/j.fct.2010.11.040
Zheng, W., Han, B., Siyu, E., Sun, Y., Li, X., Cai, Y., & Zhang, Y. N. (2020). Highly-sensitive and reflective glucose sensor based on optical fiber surface plasmon resonance. *Microchemical Journal, 157*. https://doi.org/10.1016/j.microc.2020.105010
Zheng, W. L., Zhang, Y. N., Li, L. K., Li, X. G., & Zhao, Y. (2022). A plug-and-play optical fiber SPR sensor for simultaneous measurement of glucose and cholesterol concentrations. *Biosensors and Bioelectronics, 198*, Article 113798. https://doi.org/10.1016/j.bios.2021.113798
Zyablov, A. N., & Vu Hoang, Y. (2022). Determination of sodium benzoate in liquids using a piezoelectric sensor modified by a molecularly imprinted polymer. *Journal of Analytical Chemistry, 77*(12), 1607–1611. https://doi.org/10.1134/s1061934822120176
Çimen, D., Bereli, N., Günaydın, S., & Denizli, A. (2022). Molecular imprinted nanoparticle assisted surface plasmon resonance biosensors for detection of thrombin. *Talanta, 246*, Article 123484. https://doi.org/10.1016/j.talanta.2022.123484